JOURNAL OF Applied Polymer SCIENCE

Special Issue: Bio-based Packaging

Guest Editors: José M. Lagarón, Amparo López-Rubio, and María José Fabra
Institute of Agrochemistry and Food Technology of the Spanish Council for Scientific Research

EDITORIAL

REVIEWS

RESEARCH ARTICLES

JOURNAL OF Applied Polymer SCIENCE

Special Issue: Bio-based Packaging

Guest Editors: José M. Lagarón, Amparo López-Rubio, and María José Fabra
Institute of Agrochemistry and Food Technology of the Spanish Council for Scientific Research

Impact of fermentation residues on the thermal, structural, and rheological properties of polyhydroxy(butyrate-*co*-valerate) produced from cheese whey and olive oil mill wastewater
L. Hilliou, D. Machado, C. S. S. Oliveira, A. R. Gouveia, M. A. M. Reis, S. Campanari, M. Villano and M. Majone, *J. Appl. Polym. Sci.* 2015, DOI: 10.1002/app.42818

Synergistic effect of lactic acid oligomers and laminar graphene sheets on the barrier properties of polylactide nanocomposites obtained by the in situ polymerization pre-incorporation method
J. Ambrosio-Martín, A. López-Rubio, M. J. Fabra, M. A. López-Manchado, A. Sorrentino, G. Gorrasi and J. M. Lagarón, *J. Appl. Polym. Sci.* 2015, DOI: 10.1002/app.42661

Antibacterial poly(lactic acid) (PLA) films grafted with electrospun PLA/allyl isothiocyanate fibers for food packaging
H. H. Kara, F. Xiao, M. Sarker, T. Z. Jin, A. M. M. Sousa, C.-K. Liu, P. M. Tomasula and L. Liu, *J. Appl. Polym. Sci.* 2015, DOI: 10.1002/app.42475

Poly(L-lactide)/ZnO nanocomposites as efficient UV-shielding coatings for packaging applications
E. Lizundia, L. Ruiz-Rubio, J. L. Vilas and L. M. León, *J. Appl. Polym. Sci.* 2015, DOI: 10.1002/app.42426

Effect of electron beam irradiation on the properties of polylactic acid/montmorillonite nanocomposites for food packaging applications
M. Salvatore, A. Marra, D. Duraccio, S. Shayanfar, S. D. Pillai, S. Cimmino and C. Silvestre, *J. Appl. Polym. Sci.* 2015, DOI: 10.1002/app.42219

Preparation and characterization of linear and star-shaped poly L-lactide blends
M. B. Khajeheian and A. Rosling, *J. Appl. Polym. Sci.* 2015, DOI: 10.1002/app.42231

Mechanical properties of biodegradable polylactide/poly(ether-block-amide)/thermoplastic starch blends: Effect of the crosslinking of starch
L. Zhou, G. Zhao and W. Jiang, *J. Appl. Polym. Sci.* 2015, DOI: 10.1002/app.42297

Interaction and quantification of thymol in active PLA-based materials containing natural fibers
I. S. M. A. Tawakkal, M. J. Cran and S. W. Bigger, *J. Appl. Polym. Sci.* 2015, DOI: 10.1002/app.42160

Graphene-modified poly(lactic acid) for packaging: Material formulation, processing, and performance
M. Barletta, M. Puopolo, V. Tagliaferri and S. Vesco, *J. Appl. Polym. Sci.* 2015, DOI: 10.1002/app.42252

Edible films based on chia flour: Development and characterization
M. Dick, C. H. Pagno, T. M. H. Costa, A. Gomaa, M. Subirade, A. De O. Rios and S. H. Flóres, *J. Appl. Polym. Sci.* 2015, DOI: 10.1002/app.42455

Influence of citric acid on the properties and stability of starch-polycaprolactone based films
R. Ortega-Toro, S. Collazo-Bigliardi, P. Talens and A. Chiralt, *J. Appl. Polym. Sci.* 2015, DOI: 10.1002/app.42220

Bionanocomposites based on polysaccharides and fibrous clays for packaging applications
A. C. S. Alcântara, M. Darder, P. Aranda, A. Ayral and E. Ruiz-Hitzky, *J. Appl. Polym. Sci.* 2015, DOI: 10.1002/app.42362

Hybrid carrageenan-based formulations for edible film preparation: Benchmarking with kappa carrageenan
F. D. S. Larotonda, M. D. Torres, M. P. Gonçalves, A. M. Sereno and L. Hilliou, *J. Appl. Polym. Sci.* 2015, DOI: 10.1002/app.42263

JOURNAL OF Applied Polymer SCIENCE

Special Issue: Bio-based Packaging

Guest Editors: José M. Lagarón, Amparo López-Rubio, and María José Fabra
Institute of Agrochemistry and Food Technology of the Spanish Council for Scientific Research

Structural and mechanical properties of clay nanocomposite foams based on cellulose for the food packaging industry
S. Ahmadzadeh, J. Keramat, A. Nasirpour, N. Hamdami, T. Behzad, L. Aranda, M. Vilasi and S. Desobry, *J. Appl. Polym. Sci.* 2015, DOI: 10.1002/app.42079

Mechanically strong nanocomposite films based on highly filled carboxymethyl cellulose with graphene oxide
M. El Achaby, N. El Miri, A. Snik, M. Zahouily, K. Abdelouahdi, A. Fihri, A. Barakat and A. Solhy, *J. Appl. Polym. Sci.* 2015, DOI: 10.1002/app.42356

Production and characterization of microfibrillated cellulose-reinforced thermoplastic starch composites
L. Lendvai, J. Karger-Kocsis, Á. Kmetty and S. X. Drakopoulos, *J. Appl. Polym. Sci.* 2015, DOI: 10.1002/app.42397

Development of bioplastics based on agricultural side-stream products: Film extrusion of *Crambe abyssinica*/wheat gluten blends for packaging purposes
H. Rasel, T. Johansson, M. Gällstedt, W. Newson, E. Johansson and M. Hedenqvist, *J. Appl. Polym. Sci.* 2015, DOI: 10.1002/app.42442

Influence of plasticizers on the mechanical and barrier properties of cast biopolymer films
V. Jost and C. Stramm, *J. Appl. Polym. Sci.* 2015, DOI: 10.1002/app.42513

The effect of oxidized ferulic acid on physicochemical properties of bitter vetch (*Vicia ervilia*) protein-based films
A. Arabestani, M. Kadivar, M. Shahedi, S. A. H. Goli and R. Porta, *J. Appl. Polym. Sci.* 2015, DOI: 10.1002/app.42894

Effect of hydrochloric acid on the properties of biodegradable packaging materials of carboxymethylcellulose/poly(vinyl alcohol) blends
M. D. H. Rashid, M. D. S. Rahaman, S. E. Kabir and M. A. Khan, *J. Appl. Polym. Sci.* 2015, DOI: 10.1002/app.42870

Journal of Applied Polymer Science

Synergistic effect of lactic acid oligomers and laminar graphene sheets on the barrier properties of polylactide nanocomposites obtained by the *in situ* polymerization pre-incorporation method

Jesús Ambrosio-Martín,[1] Amparo López-Rubio,[1] María José Fabra,[1] Miguel Angel López-Manchado,[2] Andrea Sorrentino,[3] Giuliana Gorrasi,[4] Jose M. Lagarón[1]

[1]Novel Materials and Nanotechnology Group, IATA-CSIC, 46980 Paterna, Valencia, Spain
[2]Institute of Polymer Science and Technology, CSIC, 28006 Madrid, Spain
[3]Institute for Polymers, Composites and Biomaterials (IPCB), National Research Council (CNR), 80055 Portici, Italy
[4]Department of Industrial Engineering, University of Salerno, Salerno, Italy
Correspondence to: G. Gorrasi (E-mail: ggorrasi@unisa.it) and J. M. Lagaron (E-mail: lagaron@iata.csic.es)

ABSTRACT: Nanocomposites of polylactide (PLA) and functionalized graphene sheets (FGS) were obtained via melt compounding. Pre-incorporation of the FGS fillers into lactic acid oligomers (OLLA) by *in situ* melt polycondensation was performed with the aim of improving the FGS dispersion and distribution into the polymeric matrix. To evaluate the effect of the pre-incorporation step, a comparison with direct addition of the filler to the melt mixing process was carried out. Addition of OLLA and FGS led to enhanced better barrier properties. Specifically, reductions of up to 45% and 41% in oxygen and water vapor permeability were achieved, respectively. Mechanical and electrical properties of the PLA and its nanocomposites were also studied and correlated with both the addition of oligomers and the incorporation method. © 2015 Wiley Periodicals, Inc. J. Appl. Polym. Sci. **2016**, *133*, 42661.

KEYWORDS: biodegradable; biopolymers & renewable polymers; composites

Received 5 May 2015; accepted 26 June 2015
DOI: 10.1002/app.42661

INTRODUCTION

One of the main functions of food packaging is the protection and preservation of food products from the adverse effects of external agents such as gases and vapors. Specifically, high barrier materials are required in packages for oxygen sensitive food products. However, plastic packages are permeable to small molecules like gases, vapors and to other low molecular weight compounds like aromas and, thus, a great deal of research has been devoted to improve the barrier properties of polymeric materials through different strategies. In fact, high barrier polymers are already being used in the food packaging field contributing to an increase in the shelf-life of foods.[1] Plastic packaging represented around 42% of the global consumption of plastic in 2011.[2] However, most of them are derived from nonrenewable petroleum-based sources which, moreover, are rarely reused or recycled, generating large volumes of residues and, thus, leading to environmental issues. Due to that, it is of great interest to develop materials for these applications based on biodegradable polymers and synthesized from renewable resources.

Poly (lactic acid) also named polylactide (PLA) is a widely studied biopolymer, attracting great interest both at the academic and industrial levels, due to its renewability and biodegradability character.[3] It is one of the most promising biopolymers to replace nonrenewable petroleum-based polymers in many applications, such as packaging, biological, and biomedical applications.[4,5] Despite of this, for high barrier applications, PLA performance needs to be improved because it has insufficient barrier to gases and vapors compared to benchmark polymers for food packaging like polyethylene terephthalate (PET), which could hardly satisfy current demands. Increasing the barrier properties of PLA would make it more competitive in the polymer market compared to conventional petroleum-based polymers.

Several strategies have been used to improve the barrier properties of PLA. As an example, blending PLA with low molecular weight lactic acid oligomers (OLLA) has been proven effective in reducing its permeability to gases and vapors (50% and 25%, respectively).[6] Furthermore, the possibility to improve the polymer barrier properties by incorporating nanofillers is one of the most widely explored strategies, being also attractive due to its low cost.[1] For instance, the incorporation of cellulose nanocrystals resulted in significantly improved barrier properties.[7–9] It is

worth mentioning that optimized dispersion of the nanofillers within the polymer matrices is crucial to obtain improved performance of the nanocomposites.[10]

Melt compounding is a polymer processing technique widely used at industrial level which can be used to incorporate nanofillers into polymer matrices. However, it has a number of drawbacks for nanocomposite development related to the high temperatures used for processing and the formation of nanofiller agglomerates during the process, regardless of the nanofiller nature.[8,9,11,12] Different strategies have been developed to improve the dispersion of the fillers through melt compounding with the aim of improving the final properties of the nanocomposites.[8,9,13–15] Among these strategies, a recently explored approach is the use of masterbatches, which could be prepared by different techniques such as *in situ* polymerization or electrospinning,[8,9] prior to the melt compounding process. Thus, preincorporation of cellulose nanocrystals in OLLA through *in situ* polymerization resulted in improved barrier properties (around 20% for both oxygen and water vapour permeability) compared with the same materials synthesized by direct addition of the filler to the melt mixing process.

Compounds with laminar structure are promising materials for improving the barrier properties of polymer matrices, as the impermeable sheets increase the tortuosity of the pathway for permeant molecules, exerting a direct effect on the diffusion phenomenon. Thus, clay nanosheets' nanocomposites have been developed demonstrating a significant impact on barrier properties.[16–20] Graphene and its derivatives, a relatively new family of compounds also with laminar geometry, have emerged in recent decades due to their excellent properties not only related to their very good mechanical and electrical properties but also to the fact that defect-free graphene sheets are impermeable to gases.[21] It is well established that these materials are highly effective for improving the barrier properties due to its planar structure.[21–23] For instance, outstanding improvements were obtained in polyphenylene sulphide/graphene nanoplatelets nanocomposites, although very high amount of fillers were necessary.[24] In addition, this family of fillers has also been already used to improve the barrier performance of PLA, reporting oxygen permeability reductions up to 45%[23] or 68%[25] for nanocomposites obtained by solution coagulation and solution casting, respectively. Moreover, Kwon *et al.* has also reported improvements in PLA oxygen barrier properties using octadecylamine–graphene oxide (ODA–GO) as filler, reaching improvements of up to 77% for 10 wt % of ODA–GO. In this case, solution intercalation was the strategy used to develop the nanocomposites. It is worth to mention that this improvement was greater than that obtained using the same amount of organically modified bentonite clay performed in the same study.[26] A similar comparison between clay and graphene nanocomposites was done by Chang *et al.*[27] which also resulted in better performance for those composites prepared with graphene due to the high aspect ratio and surface area of graphene which provided a more tortuous path. To the best of our knowledge, there is no previous study reporting on barrier improvements of PLA–graphene nanocomposites obtained through melt compounding.

In this study, graphene nanosheets have been incorporated into PLA using melt compounding. Derivative graphene material, such as functionalized graphene sheets (FGS), was used since functional sites could favor interactions with the matrix, as previously reported.[28] A comparison between direct addition of the nanofiller and the pre-incorporation of graphene in OLLA, synthesized by *in situ* polymerization, was assessed. This incorporation strategy has been recently demonstrated to be effective improving the dispersion of cellulosic fillers into PLA matrix.[9,29] The effect of the addition of these nanosheets on the thermal, mechanical, electrical, and barrier properties of the materials has been evaluated.

EXPERIMENTAL

Materials

Semicrystalline PLA was used with a number average molecular weight (M_n) of 130,000 g/mol and a weight average molecular weight (M_w) of 150,000 g/mol manufactured by NatureWorks. Lactic acid (LA) was supplied as a 90 wt % aqueous solution by Across Organics (Belgium).

Preparation of FGS

Thermal reduction of graphite oxide at 1000°C for 30 s under air atmosphere was used to synthesize FGS. Briefly, an initial dispersion of graphite powder (purum powder < 0.1 mm, Sigma Aldrich) into 20 mL of fuming nitric acid for 20 min was prepared. After that, potassium chlorate (8 g) was slowly added over 1 h, and the reaction mixture was stirred for 21 h at 0°C. The so-obtained material leads to the formation of single graphene layers or stacks of up to seven sheets with hydroxyl, carbonyl, and epoxy groups on their surface.[28] A complete description of the synthesis and characterization of the FGS can be found elsewhere.[30]

In Situ Melt Polycondensation

FGS was first swollen in the liquid monomer (LA), and the mixture was vigorous stirred overnight. The mixture was then placed in a three-necked flask equipped with mechanical stirrer, temperature controller, and a vacuum system through a cold trap. The system was initially dehydrated at 150°C and atmospheric pressure for 2 h. Subsequently, the pressure was reduced to 100 mmHg and kept during 2 h and finally at 30 mmHg and kept for another 4 h. Thus, lactic acid oligomers [(oligo(L-lactic acid, OLLA)] containing FGS nanosheets were prepared. The product was allowed to cool at room temperature, ground into powder, and washed with diethyl ether. A purified material containing oligomers and FGS (OLLA–FGS) was obtained after vacuum filtration and drying at 70°C during 24 h in a vacuum oven. The so-obtained material was used as masterbatch. The FGS content in the obtained hybrid material was determined by means of thermogravimetric analysis (TGA) under nitrogen flow (10°C/min) and it was found to be around 9 wt % of FGS. Moreover, using the aforementioned procedure but in absence of FGS, purified OLLA were also obtained.

Preparation of Films

Films composed by PLA, OLLA, and FGS were prepared by an initial melt mixing process in a Brabender Plastograph internal mixer at 162°C and 120 rpm for 5 min and subsequent

compression moulding in a hot-plate hydraulic press (165°C and 2 MPa for 2 min). After that, all films were allowed to cool at room temperature. Different contents of FGS were incorporated at weight ratios of 0.1, 0.5, 1, and 2 wt % of FGS with respect to the total amount of material. Two incorporation procedures were compared: (a) on the one hand the FGS was added from the masterbatch (PLA–FGS) and (b) on the other hand FGS was directly added to the melt mixer (PLA–FGS-D). Purified OLLA was added in all samples in order to reach a total amount of OLLA of 25 wt %. A mixture of PLA and 25 wt % of OLLA was also developed as reference material. The so-obtained films had an average thickness of about 200 μm as measured with a Mitutoyo micrometer by averaging four measurements on each sample.

Scanning Electron Microscopy

The morphological features of the different developed materials were investigated by scanning electron microscopy (SEM). The samples were immersed in liquid nitrogen and cryofractured, mounted on bevel sample holders and sputtered with Au/Pd in a vacuum. A Hitachi microscope (Hitachi S-4800) was used to perform the experiments at an accelerating voltage of 10 kV and a working distance of 12–16 mm taking pictures for the sample thickness.

Transmission Electron Microscopy

Transmission electron microscopy (TEM) was performed using a JEOL 1010 (Jeol, Tokyo, Japan) equipped with a digital Bioscan (Gatan) image acquisition system. TEM observations were performed on ultrathin sections of microtomed thin composite sheets.

Differential Scanning Calorimetry

Differential scanning calorimetry (DSC) was used to evaluate the thermal properties of PLA and its nanobiocomposites with FGS using Perkin- Elmer DSC 8000 thermal analysis system. The analysis was carried out on samples with a mass ranging between 8 and 10 mg. A heating rate of 10°C min^{-1} was used to heat the samples from 10 to 180°C using a refrigerating cooling accessory (Intracooler 2 from Perkin Elmer). The first and second melting endotherms after controlled crystallization step at 10°C min^{-1} from the melt were analyzed. Prior to the experiments, heat flow and temperature were calibrated using indium as standard. The crystallinity (%X_c) of PLA and the nanocomposites were calculated from the corrected enthalpy for biopolymer content, using the ratio between the enthalpy of the studied material and the enthalpy of a perfect PLA crystal:

$$\%X_c = \frac{(\Delta H_f - \Delta H_c)}{\Delta H_f^{\circ}(1-w)} \times 100 \quad (1)$$

where ΔH_f is the enthalpy of fusion and ΔH_c the enthalpy of cold crystallization of the studied specimen. ΔH_f° is the enthalpy of fusion of a totally crystalline material and w is the weight fraction of the filler. The ΔH_f° used for this equation was 93 J g^{-1} for PLA.[7]

Thermogravimetric Analysis

Thermal stability of materials was investigated by TGA. The tests were performed using a TGA2950 (TA Instruments) under nitrogen flow. The samples were heated from 40°C up to 800°C at 10°C min^{-1} heating rate. Derivative thermogravimetric curves (DTG) express the weight loss rate as a function of temperature.

Oxygen Transmission Rate

The oxygen permeability of the films was measured in duplicate by using an Oxtran 100 equipment (Modern Control, Minneapolis, MN) at 80% relative humidity (RH) and 24°C. RH was generated by a built-in gas bubbler and was checked with a hygrometer placed at the exit of the detector. Prior to the measurements, the samples were purged with nitrogen for a minimum of 20 h in the previously relative humidity equilibrated samples. The oxygen flow during the experiments was fixed at 10 mL min^{-1}. The measurements were performed through a 5 cm^2 sample area by using an in-house developed mask. To obtain the oxygen permeability, film thickness was considered in each case.

Water Permeability

The water vapor permeability of samples was measured by gravimetric analysis using Payne permeability cups (Elcometer SPRL, Hermelle/s Argenteau, Belgium). The samples were placed between the aluminium top (open O-ring) and bottom part (deposit for the permeant) with a Viton rubber ring between the film and the top part of the cups to enhance sealability. The cups were placed inside a desiccator at 0% RH and the water weight loss through a film area of 0.001 m^2 was monitored and plotted as a function of time. Water vapor permeation rate was estimated from the slope of the linear part of this plot, thus ensuring the steady-state conditions. Cups with aluminium films were used as control samples to estimate water vapor losses through the sealing. Water weight loss was calculated as the total cell loss minus the loss through the sealing. Water vapor permeability was obtained multiplying the water vapor permeation by the average film thickness. The tests were done at least in duplicate.

Mechanical Properties

An Instron 4400 Universal Tester equipment was used for the tensile testing. The experiments were carried out 50% RH and 24°C. Strips of samples (5 mm in width and 25 mm in length) were mounted in the tensile grips and stretched at a rate of 10 mm min^{-1} until failure. Elastic modulus (E), tensile strength, and elongation at break (ε_b) were determined from the stress–strain curves, estimated from force–deformation data. The storage conditions before test were 24°C and 0% RH. The results were taken as average of, at least, three tests.

Electrical Properties

Electrical characterization has been done, using a Keithley 2400 source measurement unit in a two-probe resistance measurement configuration. However, it should be mentioned that for some selected samples was found that four-point and two-point measurements configuration gave very similar results. The sample thicknesses were carefully measured by a micrometer, whereas the length and the width were 5 and 30 mm, respectively. The electrical conductivity was measured in the voltage range −10 + 10 V. All the samples showed a linear behavior of the current (I) versus the applied voltage (V).

RESULTS AND DISCUSSION

FGS were preincorporated into OLLA through *in situ* polymerization to obtain a masterbatch (OLLA–FGS). Different amounts of OLLA–FGS masterbatch prepared by *in situ* polymerization were blended with PLA using melt compounding to prepare samples with different FGS content. Moreover, based on previous results which demonstrated that addition of OLLA up to 25 wt % within PLA significantly improved its barrier properties,[6] in this study, the amount of total oligomers incorporated into PLA was fixed at 25 wt %. To this aim, additional OLLA to that included in the masterbatch was added to reach this content. Thus, the potential synergistic effect when adding different amounts of FGS on the final properties of the materials were evaluated.

Morphological Characterization

The dispersion of the FGS within the PLA matrix was studied using SEM and TEM. Figure 1 shows the cryofractured sections of the neat PLA and its nanocomposite films using both addition routes, that is, direct addition and with an *in situ* polymerization pre-incorporation step. An initial observation was that while for PLA and PLA–OLLA a smooth fracture surface was clearly seen, when FGS was added the surface became rougher, especially for high FGS contents. This effect has also been reported when graphene was incorporated into poly(vinylidene fluoride),[31] PLA,[32] or poly(hydroxybutyrate-co-hydroxyvalerate) (PHBV).[33] Random dispersion and distribution of the filler was generally observed for the samples obtained through a pre-incorporation method although some small aggregates were also present. On the other hand, bigger aggregates were observed when FGS was directly added to the melt mixing process, indicating that better dispersion of the FGS was obtained using the pre-incorporation step with a more intimate mixing between filler and matrix. In a previous work using the same procedure with another additive, direct addition of the filler resulted in very big agglomerates which could be seen by naked eye. This problem was overcome using the *in situ* polymerization pre-incorporation step improving to a great extent the dispersion of the filler.[9] Figure 2 shows the TEM micrographs of PLA–FGS nanocomposites containing 1 wt % of FGS synthesized through both addition routes. These images further confirm the random filler dispersion and distribution, the presence of filler agglomerates in certain areas and also bigger aggregates when FGS was directly added.

Thermal Properties of PLA and its Nanocomposites

With the aim of investigating the effects of the FGS addition on the thermal properties of the PLA nanocomposites, DSC analysis of all the samples was carried out. Glass transition temperature (T_g) and melting enthalpy (ΔH_m) normalized to the PLA content of the nanocomposite films were evaluated from the DSC first and second heating runs. Moreover, the melting temperature (T_m), degree of crystallinity (X_c), and the cold crystallization temperature (T_c) were also measured from the first heating run curve, which provided information related to the thermal characteristics of the just obtained material. Table I gathers the DSC data for PLA and its nanocomposites. The first interesting observation is that after OLLA or OLLA–FGS addition, a double melting peak appeared. It has been reported that this effect could be attributed either to a melt recrystallization mechanism or to the coexistence of two crystals size populations for PLA-based materials containing oligomers.[6] Regarding the glass transition temperature, previous studies have observed that it increased with the addition of graphene nanoplatelets or graphene oxide due to the restriction of the molecular mobility exerted by the laminar structures.[25] On the contrary, addition of OLLA to the PLA matrix resulted in a decrease in the glass transition temperature[6] due to a plasticization effect, in terms of glass transition temperature, exerted by the shorter polymer chains, which require less energy to activate molecular mobility.[34] As observed in Table I, addition of OLLA resulted in a T_g reduction of about ~6°C. Since neat PLA has

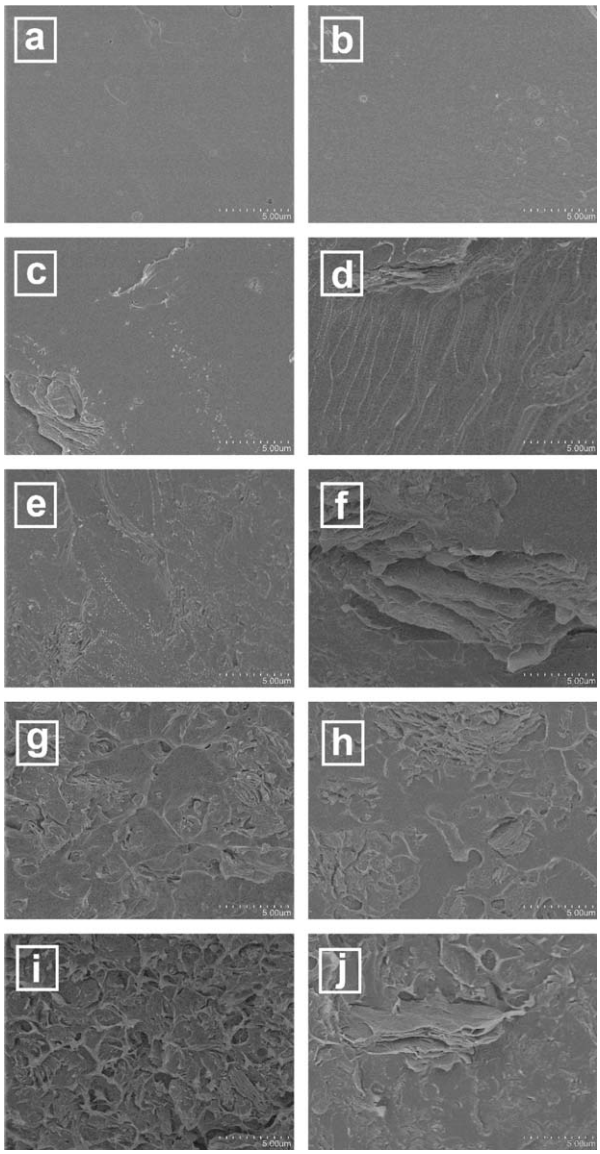

Figure 1. SEM micrographs of the cryo-fractured sections of pure PLA (a), PLA–OLLA (b), and PLA–FGS nanocomposite films at 0.1 wt % (c, d); 0.5 wt % (e, f); 1.0 wt % (g, h), and 2.0 wt % (i, j) obtained using an *in situ* polymerization step and by direct addition to the melt mixer, respectively. Scale markers correspond to 5 μm.

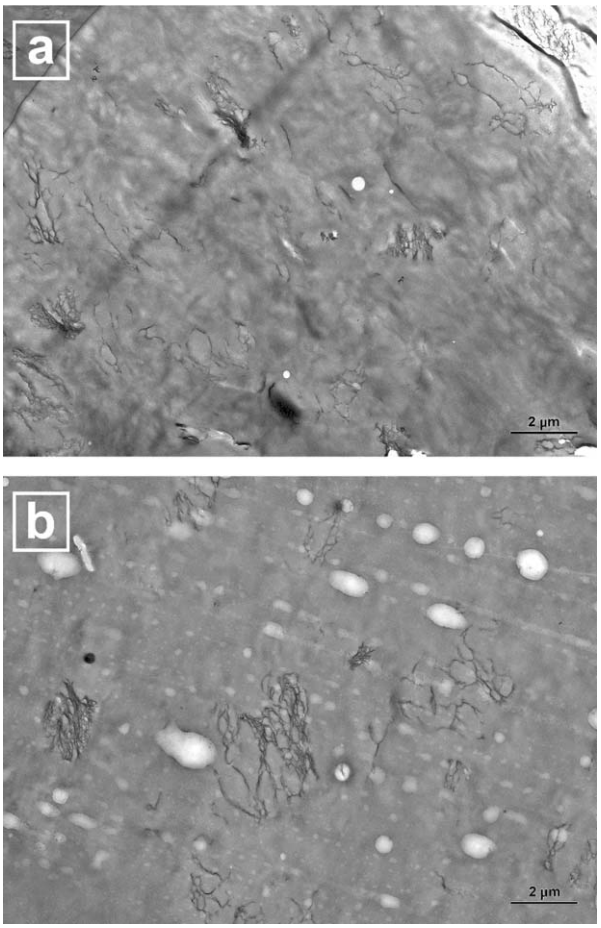

Figure 2. TEM micrographs of PLA–FGS films containing 1 wt % FGS obtained using an *in situ* polymerization step (a) and by direct addition to the melt mixer (b). Scale markers correspond to 2 μm.

different properties to these of PLA blended with oligomers, this last sample was taken as a reference. Thus, while direct addition of FGS led to a further T_g reduction of 6°C for the 2 wt % sample, when FGS was added using *in situ* melt polycondensation step, no significant differences in the glass transition temperature were observed. This could indicate that direct addition generated lower dispersion as observed in the morphological analysis and, hence, poorer filler–matrix interfacial interactions were established. Even though it was surprising that no increase in T_g was observed upon addition of FGS, even with the pre-incorporation method, similar results have been previously observed. Specifically, it was observed that addition of epoxidized palm oils enhanced the molecular motions of PLA chains, manifested by a decrease in T_g[35] and addition of graphene nanoplatelets into this plasticized system resulted in a further T_g decrease.[36] On the other hand, while differences in the glass transition temperature were observed depending on the FGS incorporation method, no significant changes in the melting temperatures were seen. Regarding the crystallization process, it is widely recognized that PLA crystallization is influenced by addition of graphene nanosheets or graphene oxide.[37–39] Table I shows a decrease in the cold crystallization temperature upon addition of FGS through both direct addition and from the masterbatch. Moreover, a sharpening of the cold

Table I. DSC Glass Transition Temperature (T_g), Maximum of Melting (T_m), and Melting Enthalpy (ΔH_m) During the First and Second Heating Run and Cold Crystallization Temperature (T_c) and Crystallinity Index (X_c) During the First Heating Run for PLA and its Nanocomposites Incorporating FGS

	First heating					Second heating	
	Tg1 (°C)	T_{m1} (°C)	T_{m2} (°C)	T_c (°C)	ΔH_m (J/g)	X_c (%)	T_{g2} (°C)	ΔH_m (J/g)
PLA	57.1 ± 0.2^{a}		147.7 ± 0.7^{a}	116.1 ± 0.0^{a}	3.2 ± 0.8^{a}	3.4 ± 0.9^{a}	58.8 ± 0.8^{a}	2.4 ± 1.0^{abc}
PLA-OLLA	51.7 ± 0.3^{b}	134.7 ± 0.7^{a}	146.4 ± 0.2^{b}	100.4 ± 0.3^{b}	2.5 ± 0.6^{a}	2.7 ± 0.7^{a}	51.6 ± 0.1^{b}	2.1 ± 1.0^{c}
PLA-FGS 0.1%	50.7 ± 0.4^{b}	134.1 ± 0.1^{b}	145.8 ± 0.0^{bc}	99.7 ± 0.2^{c}	2.4 ± 1.2^{a}	2.6 ± 1.3^{a}	49.5 ± 0.3^{d}	2.0 ± 0.4^{abc}
PLA-FGS 0.5%	49.3 ± 0.1^{bc}	133.9 ± 0.1^{b}	145.9 ± 0.2^{bc}	99.0 ± 0.2^{d}	1.8 ± 0.7^{a}	1.9 ± 0.7^{a}	49.6 ± 0.3^{cd}	2.8 ± 0.8^{abc}
PLA-FGS 1%	51.6 ± 0.9^{b}	133.8 ± 0.1^{b}	145.9 ± 0.0^{bc}	97.4 ± 0.1^{f}	2.5 ± 0.5^{a}	2.7 ± 0.6^{a}	49.4 ± 0.2^{d}	3.3 ± 1.1^{ab}
PLA-FGS 2%	51.0 ± 0.0^{b}	134.5 ± 0.0^{b}	146.3 ± 0.0^{bc}	96.9 ± 0.0^{g}	1.6 ± 0.8^{a}	1.7 ± 0.9^{a}	50.3 ± 0.1^{c}	1.6 ± 0.6^{bc}
PLA-FGS 0.1%-D	48.2 ± 0.3^{c}	133.7 ± 0.3^{b}	145.7 ± 0.2^{bc}	98.3 ± 0.1^{e}	2.6 ± 0.9^{a}	2.8 ± 1.0^{a}	49.1 ± 0.1^{de}	2.5 ± 0.5^{abc}
PLA-FGS 0.5% D	48.0 ± 0.0^{c}	134.2 ± 0.2^{b}	146.0 ± 0.1^{bc}	98.8 ± 0.2^{de}	2.2 ± 0.7^{a}	2.3 ± 0.7^{a}	48.9 ± 0.5^{de}	2.6 ± 0.5^{a}
PLA-FGS 1%-D	51.0 ± 0.6^{b}	133.8 ± 0.3^{b}	145.4 ± 0.3^{c}	98.3 ± 0.3^{e}	2.4 ± 0.7^{a}	2.6 ± 0.7^{a}	48.4 ± 0.2^{e}	2.1 ± 1.3^{abc}
PLA-FGS 2%-D	45.1 ± 1.5^{d}	133.7 ± 0.2^{b}	145.8 ± 0.5^{b}	97.8 ± 0.0^{ef}	2.2 ± 0.1^{a}	2.4 ± 0.2^{a}	48.5 ± 0.1^{e}	3.0 ± 0.8^{ab}

Different superscripts (a–g) within the same column indicate significant differences among samples ($p < 0.05$).

Table II. Maximum of the Weight Loss First Derivate Thermogravimetric Curve (T_d), the Corresponding Peak Onset Values, and the Residue at 500°C for the PLA and its Nanocomposites Films

	T_d (°C)	Onset T (°C)	Residue at 500°C (%)
PLA	357.3	323.8	2.0
PLA–OLLA	352.0	255.6	1.8
PLA–FGS 0.1	353.4	254.2	1.3
PLA–FGS 0.5	355.0	254.5	2.0
PLA–FGS 1	353.1	250.6	2.8
PLA–FGS 2	353.6	250.9	2.8
PLA–FGS 0.1-D	354.7	257.4	1.2
PLA–FGS 0.5-D	352.9	255.0	1.5
PLA–FGS 1-D	352.9	245.4	1.9
PLA–FGS 2-D	347.7	247.7	3.4

crystallization peak was obtained (results not shown). Therefore, it could be stated that the crystallization process was promoted by the addition of FGS, which acted as nucleating agent, and the nonisothermal crystallization process was accelerated. This effect has also been reported when graphene was added as nanofiller in different polymer matrices,[33,37,40,41] also including PLA matrix.[42] Nevertheless, different results were obtained depending on the FGS incorporation method used. While for direct FGS addition there were almost no differences with the amount of FGS in the nanocomposite, when FGS was added from an *in situ* polymerized masterbatch with OLLA, T_c decreased as the FGS content increased. This could be related with the morphological study where bigger aggregates were observed when FGS was directly added, impairing to some extent the nucleating effect of the FGS. This was in line with recent studies incorporating graphene into biopolymeric matrices which have also shown that good dispersion of the filler led to high nucleating effect and, hence, promoted a faster crystallization.[33,42]

The crystallinity degree was also studied to investigate whether the addition of the FGS affected the crystalline fraction of the obtained materials. Surprisingly, even though the crystallization process was promoted upon FGS addition, no significant effects on crystallinity were observed, obtaining the same crystalline fraction for all the materials regardless the addition route if compared with the reference material. However, a reduction of the crystalline fraction was obtained for all materials in comparison with pure PLA. This is in agreement with a previously reported work[6] where the addition of high amounts of OLLA into PLA resulted in a reduction of the PLA crystallinity. It seems that the nucleating character of FGS was capable to produce an effect in the initiation of the crystallization, accelerating the process, but on the contrary the high amount of OLLA hindered the growth of the crystalline fraction.

Thermal Stability of PLA and its Nanocomposites

The thermal stability of PLA and its nanocomposites with FGS was evaluated through TGA. As observed from Table II, addition of OLLA slightly affected the peak maximum of thermal degradation (T_d). However, a remarkable effect on the onset degradation temperature was observed after incorporation of OLLA, with reductions of up to ~70°C. These results are consistent with a previous study which reported that incorporation of the same amount of OLLA into PLA also induced a reduction in the onset degradation temperature, having no significant effect on the T_d.[6] This was mainly ascribed to the earlier degradation of the short oligomer chains in comparison with the onset degradation temperature of the higher molecular weight PLA. Figure 3 shows the derivative weight loss curve of pure PLA and PLA–OLLA where this decrease in the onset of degradation temperature for the material containing the oligomer is clearly observed. Whereas for pure PLA a typical one-step derivative weight loss curve was observed, a shoulder before the main degradation peak appeared when OLLA was added, indicating that the short chain oligomers degraded at lower temperatures. Generally, the addition of increasing amounts of FGS did not strongly affect the T_d of the matrix, independently of the incorporation route used. However, in the case of direct addition at 2 wt % loading a relevant reduction in the T_d was observed. It has been previously reported that addition of well dispersed nanofillers into polymeric matrices can generate a strong nanofiller network which delays thermal degradation due to the restricted polymer chains mobility.[43] Therefore, as deduced from the thermal properties analysis, in which a lower glass transition temperature was observed for the 2 wt % sample obtained by direct addition, the reduction in thermal stability could be explained by enhanced polymer chain mobility. Regarding the onset temperature, since the same amount of OLLA was present in all samples containing FGS than in the PLA–OLLA sample, the same effect was observed, that is, a remarkable reduction when compared to PLA. In addition, the incorporation of FGS had a further effect on the onset degradation temperature since lower onset temperatures were in general observed for the samples with greater FGS content, as observed in Table II. The decrease in the onset degradation temperature could be ascribed to the high thermal conductivity and low heat barrier effect of graphene in polymer composites. In fact, a recent study reported that PLA–graphene nanocomposites could be ignited with less heat irradiation than the pristine

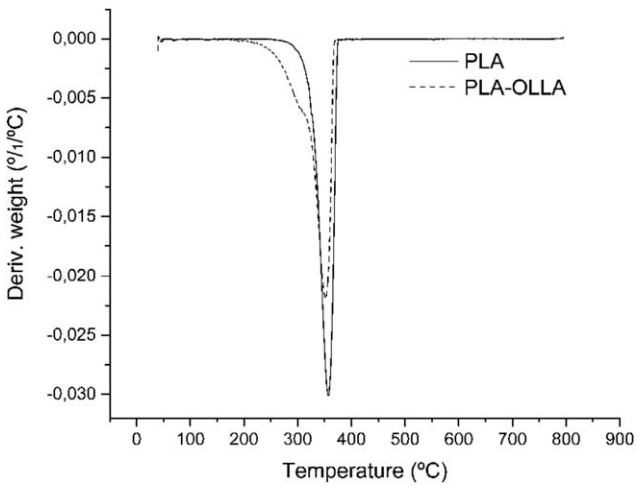

Figure 3. DTG curves of PLA and PLA–OLLA.

Table III. Elastic Modulus (E), Tensile Strength, and Elongation at Break (ε_b) for PLA and its Nanocomposites Incorporating FGS

	E (MPa)	Tensile Strength (MPa)	ε_b (%)
PLA	1670.4 ± 33.0^{cd}	61.1 ± 1.1^{a}	6.6 ± 1.2^{a}
PLA–OLLA	1701.1 ± 57.3^{c}	54.3 ± 0.8^{b}	3.9 ± 0.8^{b}
PLA–FGS 0.1	1866.0 ± 119.1^{a}	50.3 ± 2.7^{bc}	2.4 ± 0.7^{cd}
PLA–FGS 0.5	1718.0 ± 5.8^{bc}	41.9 ± 0.4^{cde}	2.1 ± 0.6^{cde}
PLA–FGS 1	1797.2 ± 100.8^{ab}	40.8 ± 5.9^{de}	2.1 ± 0.5^{cde}
PLA–FGS 2	1696.9 ± 35.2^{bc}	28.4 ± 1.3^{f}	1.5 ± 0.1^{de}
PLA–FGS 0.1-D	1461.5 ± 7.1^{e}	19.2 ± 5.4^{g}	1.3 ± 0.4^{e}
PLA–FGS 0.5-D	1514.3 ± 30.7^{d}	18.8 ± 1.0^{g}	1.4 ± 0.4^{de}
PLA–FGS 1-D	1796.4 ± 20.8^{ab}	46.2 ± 9.5^{bcd}	3.0 ± 0.2^{bc}
PLA–FGS 2-D	1717.5 ± 22.3^{bc}	32.7 ± 3.0^{ef}	1.9 ± 0.2^{cde}

Different superscripts (a–g) within the same column indicate significant differences among samples ($p < 0.05$).

polymer due to the high heat conductivity of graphene which allowed easier and faster heat diffusion through the matrix.[40] Not surprisingly, an increase in the residue at 500°C was observed as the FGS content increased. Therefore, a negative synergistic effect on the onset degradation temperature was observed upon addition of both OLLA and FGS, thus decreasing the thermal stability of neat PLA.

Mechanical Properties

The mechanical properties of PLA and its corresponding FGS-containing nanocomposite films obtained using both the masterbatch prepared through *in situ* polymerization and direct addition of the filler with the OLLA in the melt mixing process are summarized in Table III. Elastic modulus (E), tensile strength, and elongation at break (ε_b) were determined from the stress–strain curves of the different films.

It is widely recognized that addition of graphene and its derivatives within polymer matrices has an important reinforcing effect due to its own nature. Moreover, proper distribution of the filler, the interfacial interaction between polymer and filler, and also the reinforcement orientation play an important role in the final mechanical properties.[44] A depth review has been previously reported about the synthesis and characterization of grapheme–polymer nanocomposites, and it was shown that addition of graphene or its derivatives into polymer matrices had a significant effect on the mechanical properties highlighting the suitability of this kind of fillers to improve the properties of polymer matrices.[44] However, no biopolymeric matrices were studied. Nevertheless, the addition of graphene or its derivatives into biopolymeric matrices has also been studied. Thus, addition of graphene oxide and graphene nanoplatelets within PLA led to an increase in Young's modulus and in tensile strength for plasticized and unplasticized films obtained through solution casting.[25] Therefore, upon addition of FGS, a reinforcing effect due to the functionalized sites from FGS surface interacting with hydrophilic groups of PLA would be expected. From Table III, an increase in the elastic modulus was generally observed for each sample obtained from the masterbatch except for the sample with higher FGS content, which remained almost unchanged. A maximum for the elastic modulus was noticed for the sample with 0.1 wt %, decreasing with further addition of FGS. This effect has been previously observed, showing an optimum loading above which the Young's modulus decreases.[25,36] This result could be explained on the basis of the agglomeration of FGS at high contents, leading to a poorer dispersion of the filler which counteracts the reinforcement improvement. On the contrary, when FGS was incorporated by direct addition, lower values of the elastic modulus were observed for low loadings probably due to the greater agglomeration of the filler, as observed by the microscopy analysis. Despite that, further addition of FGS (up to 1 and 2 wt %) through direct incorporation resulted in an increase in the elastic modulus but without significant differences with the same compositions obtained by the pre-incorporation route. It has been recently reported that increasing the filler content leads to an enhanced contact between the nanofillers, resulting in a slight stiffening of the materials.[36] Therefore, addition of FGS at low contents by the melt polycondensation step showed better behaviour in terms of mechanical properties than those obtained by direct addition due to their better dispersion, ascribed to better filler–filler and filler–matrix interactions. However, at high FGS contents, even though the pre-incorporation step led to better nanofiller dispersion, almost no differences in mechanical properties were observed most likely due to the fact that filler aggregation occurs during both processing methods leading to less property differentiations. A previous work also reported an increase of the storage modulus in the whole temperature span calculated by dynamic mechanical analysis for nanocomposites composed by a biopolymeric matrix such as poly (3-hydroxybuturate-*co*−3-hydroxyvalerate) and the same nanofiller, that is, FGS, which corroborates the potential of this type of nanofiller for improving the mechanical properties of biopolymers.[45]

Surprisingly, an embrittlement of the materials was observed for all samples with a decrease in the tensile strength upon addition of FGS. Despite that, similar trend to that observed for the elastic modulus was noticed, that is, better tensile strength for the samples with low FGS content obtained by the pre-incorporation step, and almost no difference between both incorporation methods at high FGS contents. Chieng *et al.*[36] observed that

Table IV. Oxygen Transport Properties, Permeability (P), Diffusion (D), Solubility (S) Coefficients, and Water Permeability Coefficients (P_w) for PLA and its Nanocomposite Films Incorporating FGS

	P (80% RH) (m^3m/m^2s Pa)	D (80%RH) (m^2/s)	S (80%RH) (g/g Pa)	P_w (kg m/m^2s Pa)
PLA	$1.81 \pm 0.05\ e^{-18a}$	$2.22\ e^{-12}$	$8.17\ e^{-07}$	$1.54 \pm 0.02\ e^{-14a}$
PLA-OLLA	$1.41 \pm 0.07\ e^{-18b}$	$2.42\ e^{-12}$	$5.82\ e^{-07}$	$1.36 \pm 0.03\ e^{-14b}$
PLA-FGS 0.1	$1.34 \pm 0.00\ e^{-18bc}$	$2.34\ e^{-12}$	$5.75\ e^{-07}$	$1.30 \pm 0.02\ e^{-14c}$
PLA-FGS 0.5	$1.25 \pm 0.02\ e^{-18cd}$	$2.20\ e^{-12}$	$5.66\ e^{-07}$	$1.18 \pm 0.01\ e^{-14e}$
PLA-FGS 1	$1.06 \pm 0.03\ e^{-18f}$	$1.95\ e^{-12}$	$5.42\ e^{-07}$	$1.10 \pm 0.02\ e^{-14f}$
PLA-FGS 2	$1.01 \pm 0.04\ e^{-18f}$	$1.66\ e^{-12}$	$6.09\ e^{-07}$	$0.91 \pm 0.00\ e^{-14h}$
PLA-FGS 0.1-D	$1.35 \pm 0.03\ e^{-18bc}$	$2.18\ e^{-12}$	$6.19\ e^{-07}$	$1.24 \pm 0.03\ e^{-14cd}$
PLA-FGS 0.5-D	$1.26 \pm 0.01\ e^{-18\ cd}$	$2.23\ e^{-12}$	$5.65\ e^{-07}$	$1.20 \pm 0.01\ e^{-14d}$
PLA-FGS 1-D	$1.20 \pm 0.06\ e^{-18de}$	$2.09\ e^{-12}$	$5.72\ e^{-07}$	$1.13 \pm 0.03\ e^{-14f}$
PLA-FGS 2-D	$1.10 \pm 0.08\ e^{-18ef}$	$1.93\ e^{-12}$	$5.71\ e^{-07}$	$1.03 \pm 0.00\ e^{-14g}$

Different superscripts (a–h) within the same column indicate significant differences among samples ($p < 0.05$).

lower tensile strength values were obtained when increasing the graphene nanoplatelets content in the PLA matrix, which was explained by their stacking above the optimum nanofiller content due to Van der Waals forces. However, in the case of direct addition of the FGS, somewhat higher values of tensile strength were obtained at high filler contents. This could be explained since at low contents higher stacking of FGS was present in samples from direct addition which resulted in lower tensile strength. On the contrary, at high contents, stacking of FGS was also present in samples obtained from the masterbatch which may lead to similar values in tensile strength for both incorporation routes, as observed in the mechanical modulus.

Addition of up to 25 wt % of oligomers had an important effect regarding the level of interaction between polymer and filler, hindering proper filler–matrix interaction. In fact, in a previous work incorporating nanocellulose using a masterbatch obtained from *in situ* polycondensation with LA, increasing the amount of oligomers resulted in a reduction in the mechanical properties explained by the reduced filler–matrix adhesion.[9] Regarding the ductility of the materials, a reduction was noticed with a decrease in the elongation at break after addition of OLLA. Further decrease was observed for all samples after addition of FGS, regardless of FGS content. Thus, the main remarkable conclusion from the mechanical tensile tests is that addition of high amounts of OLLA into PLA hindered to a great extent the reinforcing effect that could be expected by FGS addition, mainly due to the short-chain feature of the oligomers and also to the highly disturbed filler–matrix interactions.

Barrier Properties

Graphene and its derivatives are considered promising nanomaterials in terms of gas and vapor barrier applications because their laminar structure can potentially block the diffusion of small molecules. The use of these materials in barrier polymers has been studied to some extent. Although a thorough revision about the topic was carried out by Yoo *et al.*,[21] there is scarce literature about the improvements in PLA barrier properties using this type of carbonaceous materials[23,25] and even less for PLA–graphene or graphene derivatives-based nanocomposites prepared by melt compounding. Oxygen transport properties including permeability (P), diffusion (D) and solubility (S), and water vapor permeability (P_w) of PLA and its nanocomposites were measured and the results summarized in Table IV.

Figure 4a shows the oxygen barrier properties of PLA and their nanocomposites with FGS. The permeability value for pure PLA was in accordance with that reported in the literature for melt

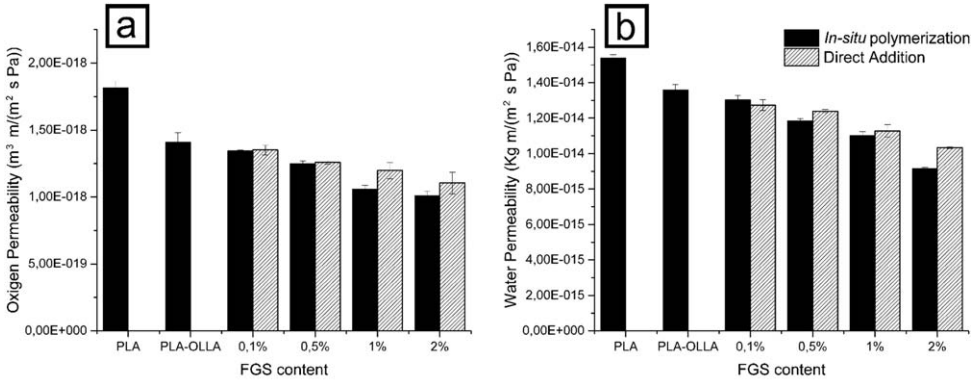

Figure 4. Oxygen (a) and water permeability (b) of pure PLA and its nanocomposites with FGS obtained using an *in situ* polymerization step and by direct addition to the melt mixer.

compounded films.[8] Moreover, addition of OLLA resulted in a reduction of the oxygen permeability of about 22%, which was in agreement with a previous work.[6] It is worthy to highlight that further reductions in oxygen permeability were obtained for all the nanocomposite materials obtained through both incorporation routes when compared to the reference sample. Even though no differences between both routes were observed at low FGS contents, at high contents, somewhat higher oxygen barrier performance was obtained for *in situ* polymerized FGS, with the greatest improvement of about 45% for the 2 wt % nanofiller loading.

There are several factors that influence the oxygen barrier properties, such as relative humidity, tortuosity of the pathway for the permeant molecules to diffuse through the polymer and the free volume of the polymer matrix, among others. It has been reported that the presence of reactive hydrophilic groups, such as hydroxyl groups from the polymer or polymer nanocomposites, can cause plasticization of the material when exposed to high relative humidity conditions due to the interaction of water with these groups, thus resulting in a higher mobility of the polymer chains and hence easing gas diffusion.[8,46] Moreover, it is widely known that an increase in tortuosity, due to nanofillers and/or crystals, translates into a reduction in the vapor and gases permeability values by a drop in diffusion, and changes in free volume, for example, amorphous density, are closely related with changes in the transport of low molecular weight compounds. Several works have demonstrated reductions in gas permeability associated with fractional free volume occupancy phenomena in polymers.[47,48]

In this study, addition of OLLA led to an increase of the hydrophilic groups which resulted in a slight increment in the diffusion coefficient when compared with PLA. Nevertheless, a strong effect on the free volume occupancy by oligomer molecules was observed with a considerable reduction in the solubility coefficient, in agreement with previous works.[6] Regardless of the incorporation route, addition of FGS resulted in a further reduction of the diffusion coefficient compared to the reference sample (i.e., PLA–OLLA), reaching even lower values than those for pure PLA. This could mainly be ascribed to the effective blocking effect of the FGS laminar sheets, resulting in an increase in tortuosity. It is widely known that an increase in polymer crystallinity is also closely related to improved barrier properties, as the crystalline domains are considered impermeable to the pass of low molecular weight compounds, thus increasing the tortuous path for the permeant molecules to go through.[49–52] A recent study has demonstrated the high "filler barrier efficiency" of this kind of fillers.[45] This "filler barrier efficiency" factor is intended to separate the effect of filler loading from crystallinity variations in the barrier performance of the materials. As observed in thermal analysis, no effect on the crystallization degree was observed upon addition of FGS, thus corroborating the very good filler barrier efficiency of these nanofillers. In fact, the higher the FGS addition, the higher the tortuosity effect observed, with greater drops in the diffusion coefficient. The higher oxygen permeability obtained for the highly loaded samples prepared from direct addition of FGS in comparison with the same compositions obtained by *in situ* polymerization could be explained by the general poorer dispersion of the nanofiller in the former samples, thus resulting in high diffusion coefficients due to creation of preferential pathways for the oxygen molecules to pass. Water permeability was also measured and the results are depicted in Figure 4b.

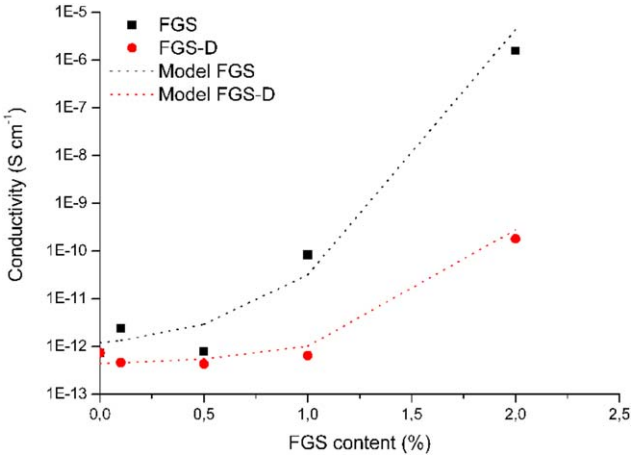

Figure 5. Experimental and calculated electrical conductivity versus filler loading for PLA–FGS nanocomposites. [Color figure can be viewed in the online issue, which is available at wileyonlinelibrary.com.]

Addition of oligomers also resulted in a reduction of the water permeability achieving an improvement of about 12%, which was in line with previous results.[6] Moreover, addition of FGS caused a greater reduction in the water permeability coefficient for all samples regardless of the FGS incorporation route. The effect of dispersion of FGS into PLA matrix was also noticed. While at low contents there were no significant differences between both incorporation routes, high FGS contents led to higher water vapor permeability for the materials synthesized by direct addition, mainly ascribed to preferential paths created by the agglomerated nanofiller. Hence, the maximum reduction in water permeability was achieved for the sample with 2 wt % FGS obtained from an *in situ* polymerized material with an improvement of about 41%, thus confirming the improved nanofiller dispersion obtained through this incorporation route.

Electrical Properties

Conductive carbonaceous materials such as carbon nanotubes, graphite, graphene and/or its derivatives have been widely used as nanofillers to improve the electrical properties of polymeric matrices.[12,24,53–56] The dispersion of the filler into de polymeric matrix plays a key role in order to obtain good results. Figure 5 shows the electrical conductivities of PLA and its nanocomposites. Neat PLA is electrically insulating with a low conductivity, which is considered to be in the range of 10^{-16} to 10^{-19} S cm^{-1} by Sullivan *et al.*[57] As observed from Figure 5, addition of conducting graphene nanofillers significantly increased the conductivity of the materials. It is reported that S-shaped curves indicate that the nanocomposites exhibit a typical percolation transition from an insulator to semiconductor.[58,59] Although it is not the case, it can be noticed the beginning of this typical S-shaped curve, with an exponential increase of the electrical conductivity, suggesting that there is a transition from insulator material to semiconductor. However, higher amounts of FGS

would be necessary to obtain the whole curve. In spite of this, differences between both incorporation routes were noticed. Higher conductivity was obtained for the nanocomposites obtained through a pre-incorporation step than that obtained through direct addition of the filler. As previously commented, the dispersion of the filler is an important factor for the electrical properties. Thus, the better FGS dispersion obtained using the pre-incorporation step could be responsible of creating more continuous conductive pathways, thus resulting in higher conductivity. However, although an increase in the conductivity was noticed when FGS nanofiller was added, the increments were not as high as expected. The low conductivity of the materials could be explained by an insufficient dispersion of the nanofiller, combined with the very low crystallinity of the polymer matrix. In fact, it has been reported that there is a strong correlation between the crystallization degree of the polymeric matrix and the electrical conductivity of the polymeric nanocomposites.[57] Samples with higher crystallinity lead to a higher electrical conductivity due to the decreased scattering of electrons through the crystalline lamella. An analytical model has been previously proposed, based on the Fermi-Dirac distribution, to describe the critical insulator to conductor transition.[60]

$$\log(\sigma_c) = \log(\sigma_f) + \frac{\log\left(\frac{\sigma_p}{\sigma_f}\right)}{(1+\exp(t(\varphi-\varphi_c)))} \quad (2)$$

where σ_c, σ_f, and σ_p are the composite, filler, and polymer conductivities, respectively, ϕ is the FGS mass fraction and t is an empirical parameter that leads to the change in conductivity at the percolation threshold ϕ_c. By assuming a constant value for σ_f and σ_p, from eq. (1) the best fitted values of ϕ_c and t were obtained. Thus, the percolation threshold value of nanocomposites was calculated at about 1 wt % for the samples produced from the masterbatch and ~2.8 wt % for the samples obtained by direct addition of the filler to the melt mixer. These percolation threshold values are in the range of the values reviewed by Galpaya *et al.*[44] for graphene (or its derivatives) nanocomposites using different polymer matrices and different incorporation routes. Again, due to the relatively bad dispersion of the filler when added directly, an increase in the percolation threshold value was obtained.

CONCLUSIONS

Nanocomposites of PLA and FGS were successfully developed through a melt compounding method. To improve the dispersion of the filler within the PLA matrix, a pre-incorporation method based on *in situ* polymerization of FGS with OLLA was used, obtaining a masterbatch material. Microscopic analysis revealed the efficiency of this pre-incorporation step to improve the dispersion of FGS into PLA if compared by that observed for the samples obtained by direct addition of the FGS to the melt mixing process. Although thermal properties were not extensively affected upon addition of FGS into PLA, a decrease in the glass transition temperature, mainly ascribed to the oligomers addition, and also, an acceleration of the crystallization process due to the nucleating effect of FGS were observed. Moreover, the thermal stability was affected after the incorporation of OLLA and FGS, with a remarkable reduction in the onset degradation temperature, due one hand to the earlier degradation of the oligomers and on the other hand to the high heat conductivity of the FGS. As expected, improved barrier properties to both oxygen and water were obtained due to the blocking effect exerted by the laminar FGS and also to the occupancy of the free volume by the oligomers molecules, which led to improvements of up to 45% and 41% in oxygen and water vapour permeability, respectively. Addition of FGS simultaneously with OLLA impaired, to some extent, the filler–matrix interactions, counteracting the expected improvement in mechanical properties. Nevertheless, an optimum in the elastic modulus was obtained for the 0.1 wt % sample obtained from the masterbatch. Lower improvements than expected were obtained in the electrical properties of the PLA nanocomposites after FGS addition, mainly due to most likely still incomplete dispersion and distribution of the filler together with the very low crystallinity of the polymeric material.

ACKNOWLEDGMENTS

J. Ambrosio-Martín would like to thank the Spanish Ministry of Economy and Competitiveness for the FPI grant BES-2010–038203. M.J. Fabra is recipient of a "Juan de la Cierva" contract from the Spanish Ministry of Economy and Competitiveness. The authors acknowledge financial support from the MINECO (MAT2012–38947-C02-01 project) and from the FP7 ECOBIOCAP project.

REFERENCES

1. Siracusa, V. *Int. J. Polym. Sci.* **2012**, *1*.
2. Silvestre, C.; Duraccio, D.; Cimmino, S. *Progr. Polym. Sci.* **2011**, *36*, 1766.
3. Auras, R.; Harte, B.; Selke, S. *Macromol. Biosci.* **2004**, *4*, 835.
4. Slomkowski, S.; Penczek, S.; Duda, A. *Polym. Adv. Technol.* **2014**, *25*, 436.
5. Oh, J. K. *Soft Matter* **2011**, *7*, 5096.
6. Ambrosio-Martín, J.; Fabra, M. J.; Lopez-Rubio, A.; Lagaron, J. M. *J. Mater. Sci.* **2014**, *49*, 2975.
7. Sanchez-Garcia, M. D.; Lagaron, J. M. *Cellulose* **2010**, *17*, 987.
8. Martínez-Sanz, M.; Lopez-Rubio, A.; Lagaron, J. M. *Biomacromolecules* **2012**, *13*, 3887.
9. Ambrosio-Martín, J.; Fabra, M. J.; Lopez-Rubio, A.; Lagaron, J. M. *Cellulose* **2015**, *22*, 1201.
10. Ramanathan, T.; Abdala, A. A.; Stankovich, S.; Dikin, D. A.; Herrera-Alonso, M.; Piner, R. D.; Adamson, D. H.; Schniepp, H. C.; Chen, X.; Ruoff, R. S.; Nguyen, S. T.; Aksay, I. A.; Prud'homme, R. K.; Brinson, L. C. *Nat. Nanotechnol.* **2008**, *3*, 327.
11. Moniruzzaman, M.; Winey, K. I. *Macromolecules* **2006**, *39*, 5194.
12. Potts, J. R.; Dreyer, D. R.; Bielawski, C. W.; Ruoff, R. S. *Polymer* **2011**, *52*, 5.
13. Pötschke, P.; Bhattacharyya, A. R.; Janke, A.; Pegel, S.; Leonhardt, A.; Täschner, C.; Ritschel, M.; Roth, S.; Hornbostel, B.; Cech, J. *Fullerenes Nanotubes Carbon Nanostruct.* **2005**, *13*, 211.

14. Annala, M.; Lahelin, M.; Seppälä, J. *Expr. Polym. Lett.* **2012**, *6*, 814.
15. Ayana, B.; Suin, S.; Khatua, B. B. *Carbohydr. Polym.* **2014**, *110*, 430.
16. Al-Qadhi, M.; Merah, N. *Polym. Compos.* **2014**, DOI: 10.1002/pc.23109.
17. Hosseinkhanli, H.; Aalaie, J.; Abdollahi, M.; Khalkhali, T.; Shojaei, M. *J. Vinyl Additive Technol.* **2015**, *21*, 60.
18. Tentschert, J.; Jungnickel, H.; Reichardt, P.; Leube, P.; Kretzschmar, B.; Taubert, A.; Lucha, A. *Surf. Interface Anal.* **2014**, *46*, 334.
19. Ojijo, V.; Ray, S. S. *Progr. Mater. Sci.* **2014**, *62*, 1.
20. Sanchez-Garcia, M. D.; Lagaron, J. M. *J. Appl. Polym. Sci.* **2010**, *118*, 188.
21. Yoo, B. M.; Shin, H. J.; Yoon, H. W.; Park, H. B. *J. Appl. Polym. Sci.* **2014**, 131.
22. Kim, H.; Abdala, A. A.; Macosko, C. W. *Macromolecules* **2010**, *43*, 6515.
23. Huang, H. D.; Ren, P. G.; Xu, J. Z.; Xu, L.; Zhong, G. J.; Hsiao, B. S.; Li, Z. M. *J. Membr. Sci.* **2014**, *464*, 110.
24. Jiang, X.; Drzal, L. T. *J. Power Sources* **2012**, *218*, 297.
25. Pinto, A. M.; Cabral, J.; Tanaka, D. A. P.; Mendes, A. M.; Magalhães, F. D. *Polym. Int.* **2013**, *62*, 33.
26. Kwon, K.; Chang, J. H. *Polymer* **2014**, *38*, 232.
27. Chang, C. H.; Huang, T. C.; Peng, C. W.; Yeh, T. C.; Lu, H. I.; Hung, W. I.; Weng, C. J.; Yang, T. I.; Yeh, J. M. *Carbon* **2012**, *50*, 5044.
28. Schniepp, H. C.; Li, J. L.; Mcallister, M. J.; Sai, H.; Herrera-Alonson, M.; Adamson, D. H.; Prud'homme, R. K.; Car, R.; Seville, D. A.; Aksay, I. A. *J. Phys. Chem. B* **2006**, *110*, 8535.
29. Xiao, L.; Mai, Y.; He, F.; Yu, L.; Zhang, L.; Tang, H.; Yang, G. *J. Mater. Chem.* **2012**, *22*, 15732.
30. Verdejo, R.; Barroso-Bujans, F.; Rodriguez-Perez, M. A.; De Saja, J. A.; Lopez-Manchado, M. A. *J. Mater. Chem.* **2008**, *18*, 2221.
31. El Achaby, M.; Arrakhiz, F. Z.; Vaudreuil, S.; Essassi, E. M.; Qaiss, A.; Bousmina, M. *J. Appl. Polym. Sci.* **2013**, *127*, 4697.
32. Kim, I. H.; Jeong, Y. G. *J. Polym. Sci., Part B: Polym. Phys.* **2010**, *48*, 850.
33. Ambrosio-Martín, J.; Gorrasi, G.; López-Rubio, A.; Fabra, M. J.; Mas, L. C.; López-Manchado, M. A.; Lagaron, J. M. *J. Appl. Polym. Sci.* **2015**, *132*, 42101.
34. Sedlarik, V.; Kucharczyk, P.; Kasparkova, V.; Drbohlav, J.; Salakova, A.; Saha, P. *J. Appl. Polym. Sci.* **2010**, *116*, 1597.
35. Giita Silverajah, V. S.; Ibrahim, N. A.; Md Zin Wan Yunus, W.; Hassan, H. A.; Woei, C. B. *Int. J. Mol. Sci.* **2012**, *13*, 5878.
36. Chieng, B. W.; Ibrahim, N. A.; Wan Yunus, W. M. Z.; Hussein, M. Z.; Loo, Y. Y. *J. Therm. Anal. Calorim.* **2014**, *118*, 1551.
37. Wu, D.; Cheng, Y.; Feng, S.; Yao, Z.; Zhang, M. *Ind. Eng. Chem. Res.* **2013**, *52*, 6731.
38. Chen, Y.; Yao, X.; Gu, Q.; Pan, Z. *J. Polym. Eng.* **2013**, *33*, 163.
39. Wang, H.; Qiu, Z. *Thermochim. Acta* **2012**, *527*, 40.
40. Bao, C.; Song, L.; Xing, W.; Yuan, B.; Wilkie, C. A.; Huang, J.; Guo, Y.; Hu, Y. *J. Mater. Chem.* **2012**, *22*, 6088.
41. Sridhar, V.; Lee, I.; Chun, H. H.; Park, H. *Expr. Polym. Lett.* **2013**, *7*, 320.
42. Manafi, P.; Ghasemi, I.; Karrabi, M.; Azizi, H.; Ehsaninamin, P. *Soft Mater.* **2014**, *12*, 433.
43. Yu, H. Y.; Qin, Z. Y.; Liu, Y. N.; Chen, L.; Liu, N.; Zhou, Z. *Carbohydr. Polym.* **2012**, *89*, 971.
44. Galpaya, D.; Wang, M.; Liu, M.; Motta, N.; Waclawik, E. R.; Yan, C. *Graphene* **2012**, *1*, 30.
45. Ambrosio-Martín, J.; Gorrasi, G.; Lopez-Rubio, A.; Fabra, M. J.; Mas, L. C.; López-Manchado, M. A.; Lagaron, J. M. *J. Appl. Polym. Sci.* **2015**, *132*, 42217.
46. Mokwena, K. K.; Tang, J. *Crit. Rev. Food Sci. Nutr.* **2012**, *52*, 640.
47. Larocca, N. M.; Pessan, L. A. *J. Membr. Sci.* **2003**, *218*, 69.
48. Maeda, Y.; Paul, D. R. *J. Polym. Sci., Part B: Polym. Phys.* **1987**, *25*, 1005.
49. Colomines, G.; Ducruet, V.; Courgneau, Ć.; Guinault, A.; Domenek, S. *Polym. Int.* **2010**, *59*, 818.
50. Kanehashi, S.; Kusakabe, A.; Sato, S.; Nagai, K. *J. Membr. Sci.* **2010**, *365*, 40.
51. Tsuji, H.; Okino, R.; Daimon, H.; Fujie, K. *J. Appl. Polym. Sci.* **2006**, *99*, 2245.
52. Komatsuka, T.; Kusakabe, A.; Nagai, K. *Desalination* **2008**, *234*, 212.
53. De Vivo, B.; Lamberti, P.; Tucci, V.; Guadagno, L.; Vertuccio, L.; Vittoria, V.; Sorrentino, A. *Adv. Polym. Technol.* **2012**, *31*, 205.
54. Gorrasi, G.; Sorrentino, A. *Polym. Degrad. Stabil.* **2013**, *98*, 963.
55. Gorrasi, G.; Milone, C.; Piperopoulos, E.; Lanza, M.; Sorrentino, A. *Appl. Clay Sci.* **2013**, *71*, 49.
56. Mittal, G.; Dhand, V.; Rhee, K. Y.; Park, S. J.; Lee, W. R. *J. Ind. Eng. Chem.* **2015**, *21*, 11.
57. Sullivan, E. M.; Oh, Y. J.; Gerhardt, R. A.; Wang, B.; Kalaitzidou, K. *J. Polym. Res.* **2014**, 21.
58. Wu, H.; Zhao, W.; Chen, G. *J. Appl. Polym. Sci.* **2012**, *125*, 3899.
59. Wu, H.; Zhao, W.; Hu, H.; Chen, G. *J. Mater. Chem.* **2011**, *21*, 8626.
60. Gorrasi, G.; Di Lieto, R.; Patimo, G.; De Pasquale, S.; Sorrentino, A. *Polymer* **2011**, *52*, 1124.